Coastal Dynamics 2013
Paper No.

INDIVIDUAL WAVE CELERITY IN THE SURF ZONE OF A LOW-SLOPING LABORATORY BEACH

Marion Tissier[1], Rafael Almar[2], Philippe Bonneton[3], Hervé Michallet[4], Florent Birrien[3], Anouk de Bakker[1] and Gerben Ruessink[1]

Abstract

A good prediction of wave celerity is essential for wave propagation modeling in the nearshore. Previous studies have been focusing on the analysis of wave celerities averaged over several waves, neglecting the intra-wave variability due to long-wave transformation for instance. This paper is devoted to a study of individual wave transformation in the surf zone of a low-sloping beach, based on the analysis of a high-resolution laboratory dataset. The variability of the individual wave celerity in the surf zone is quantified and is seen to relate with the local elevation of the long waves normalized by the mean water depth. Lastly, individual wave celerities are compared to the predictions given by several linear and non-linear models.

Key words: Broken wave celerity, infragravity waves, bore merging, non-linear celerity predictors

1. Introduction

A good prediction of the celerity of a broken wave is essential, as it is a key parameter for nearshore wave propagation models. In phase-averaged models for instance, the parameterization of the celerity will determine the mass flux, the energy flux and the energy dissipation. A better understanding of wave celerity is also important for the development of remote sensing techniques. In depth-inversion techniques for instance, the accuracy of the results directly depends on the knowledge of a good relationship between wave celerity and water depth (see for instance Holland, 2001, Catalan and Haller, 2008, Almar *et al.*, 2008). This accuracy has been found to significantly degrade in the surf zone, where wave dynamics become increasingly non-linear.

Common approaches to describe broken wave celerity rely on the assumption of a given (fixed) wave shape, or at least a slowly varying one, while the surf-zone is characterized by highly non-stationary dynamics. Predictors derived from linear wave theory are often used. Several studies have shown that they could only give a rough estimate of the broken wave celerity averaged over many waves (e.g., Holland, 2001). Taking into account non-linear effects, essential in surf zone dynamics, leads to improved predictions, but significant discrepancies still remain. Recent studies (e.g., Tissier *et al*., 2011) have shown that the main discrepancies were found in very shallow water, just seaward of the swash zone. In particular, it has been shown that the classical bore model (Svendsen *et al*., 1978), which is the most commonly-used non-linear celerity predictor, was inappropriate to describe wave dynamics when approaching the swash zone.

The relatively poor description of wave celerity in the surf zone results also from methodological limitations. Previous studies devoted to broken wave celerity were based on the evaluation of bulk values (e.g. Thornton and Guza, 1982; Catalan and Haller, 2008; Tissier *et al.,* 2011). A representative celerity was estimated over a large number of waves, and related to averaged wave properties. The intra-wave variability was therefore not accounted for. However, in shallow water, a large variability of the wave field both in time and space can be observed, due to the presence of (long) infragravity waves for instance. These long waves, often energetic close to the shore, can strongly modulate water depth and velocity and induce local

[1]Dept. Physical Geography, Faculty of Geosciences, Utrecht University, Netherlands. m.f.s.tissier@uu.nl, a.t.m.debakker@uu.nl, b.g.ruessink@uu.nl
[2]IRD-LEGOS (CNES/CNRS/IRD-University of Toulouse), Toulouse, France. rafael.almar@ird.fr
[3]UMR EPOC, Université de Bordeaux I, France. p.bonneton@epoc.u-bordeaux1.fr
[4]LEGI, University of Grenoble, France. herve.michallet@legi.grenoble-inp.fr

changes in short-wave celerity. In this paper, we perform a wave-by-wave analysis of celerity based on the analysis of a high-resolution (in space and time) dataset of surface elevation collected in the framework of the EU-Hydralab IV GLOBEX laboratory experiment. We first analyze the transformation of the individual short-waves while they propagate towards the shore, in terms of individual wave characteristics and celerity. We then quantify and analyze the observed dispersion of individual wave celerity in shallow water. Finally, the observed celerities are compared with several linear and non-linear celerity predictors.

2. Laboratory data and method

2.1. *Presentation of the dataset*

The GLOBEX laboratory experiment was conducted in the 110-m long Scheldegoot flume at Deltares to investigate short- and long-wave propagation and interaction over a very low-sloping (1:80) beach (Ruessink *et al.,* 2013). Eight wave conditions were considered during this experiment (3 random, 3 bichromatic and 2 monochromatic cases), and were repeated 10 times for different instrument positions. This resulted in a total of 190 measurement locations for the free-surface elevation and 43 for the velocity per wave condition, recorded with a sampling frequency F_s=128 Hz. Within the surf and swash zones, cross-shore arrays of 52 to 93 synchronized capacitance gauges are available, depending on the incoming wave conditions. Further details concerning the experimental set-up can be found in Ruessink *et al*. (2013).
In this paper, we focus on the analysis of the three bichromatic cases, particularly suited for the study of wave celerity because the regular groups allow for ensemble averaging and, hence, more robust statistics compared to the random-wave cases. The incoming wave characteristics for the 3 cases considered in this paper can be found in Table 1.

Table 1 Wave conditions for the bichromatic cases (f_1 and f_2 primary frequencies, a_1 and a_2, associated amplitudes)

	a_1 (m)	a_2 (m)	f_1 (Hz)	f_2 (Hz)
B1	0.09	0.01	6/15	7/15
B2	0.09	0.01	0.42	0.462
B3	0.07	0.03	0.42	0.462

2.2. *Computation of wave celerity*

The time-series of free-surface elevation were first averaged over the group and combined in a time-space diagram (see examples in Fig. 1). The estimation of individual wave celerity was then based on a simple crest-tracking method. The crests belonging to one wave group were identified at the most offshore location as the local maxima of free-surface elevation and followed during their propagation toward the shore. The only assumption made to track the crests from one location to the next one is that their propagation speed c was such as $0.2(gh_m)^{1/2} < c < 2(gh_m)^{1/2}$, with h_m the water depth averaged over the entire time-series. Figure 1 shows the trajectories resulting from our crest tracking procedure for the cases B1 (6 waves per group) and B3 (10 waves per group). The celerities were finally computed as the derivative of these trajectories ($c = \mathrm{d}x_c/\mathrm{d}t$). This simple methodology gives reliable results for the bichromatic cases after ensemble averaging, but will be less straightforward to apply for random wave cases. Other approaches to estimate individual wave celerities, such as the Radon Transform presented in Almar *et al.* (2013), should be used to study more complicated cases.
Bulk estimates of the celerity were also computed for validation purposes using the cross-correlation method introduced in Tissier *et al*. (2011). For the computation of the cross-correlations, we consider 2-minute long free-surface elevation time-series distant from 40 to 80 cm.

2.3. *Estimation of individual wave characteristics*

To analyze the celerity data, it is necessary to precisely define the characteristics of the individual waves. For each wave and at each location, the wave trough is defined as the first local minimum of free-surface elevation preceding the crest. The wave height is then computed as the difference of free-surface elevation between crest and trough. The wave period is estimated as the time separating the crests of two consecutive waves.

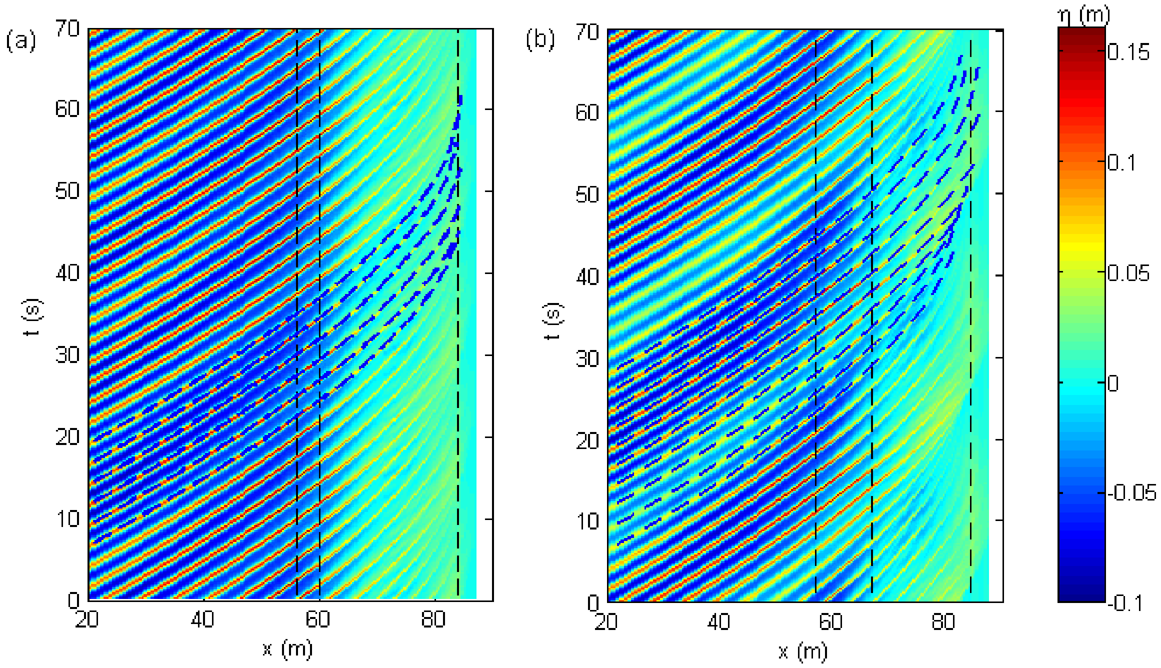

Figure 1: Space-time diagram of ensemble averaged free-surface elevation measured during B1 (a) and B3 (b). The thick dashed lines represent the wave trajectories used to compute celerity. The vertical dashed lines represent (from left to right) the position where the largest waves start breaking, the position where the smallest waves start breaking, and the start of the swash zone (maximum run-down). These positions were determined visually during the experiments.

Lastly, we define the water depth h_{loc} in which each wave locally propagates. To this end, the total water depth time-series is decomposed as:

$$h = d + \overline{\eta} + \eta_{hf} + \eta_{lf}, \qquad (1)$$

with d the water depth at rest, and $\overline{\eta}$, η_{hf} and η_{lf} the mean (set-up), high frequency, and low frequency part of the free-surface elevation time-series (with respect to the water level at rest). To separate the low and high frequency parts of the signal, we choose $f_{cut} = f_2/2$. The water depth h_{loc} is then defined as the average value of the low-pass filtered water depth ($d + \overline{\eta} + \eta_{lf}$) over the wave front.

3. Data analysis

3.1. *Short-wave transformation*

The individual wave periods T, heights H and relative wave heights H/h_{loc} are presented in Figure 2 for the three experimental conditions introduced in Table 1. In this figure, each line represents the cross-shore evolution of a parameter for a given wave. The variability of the individual wave periods (Figs. 2*a*,*d*,*g*) increases sharply when entering the surf zone, suggesting an increased variability of the intra-wave celerity after the breaking point. These variations are the result of the crest convergence/divergence observed in shallow water (see also time-stacks in Fig. 1). The largest variations of the individual wave periods can be found in case B3, which corresponds to the wave conditions with the largest low-frequency modulation of the incoming wave field (see Table 1). In this case, some crests end up merging (T drops to zero, see also Fig.1*b*, x=80 m), reducing the amount of waves at a given location and therefore considerably increasing the mean period.

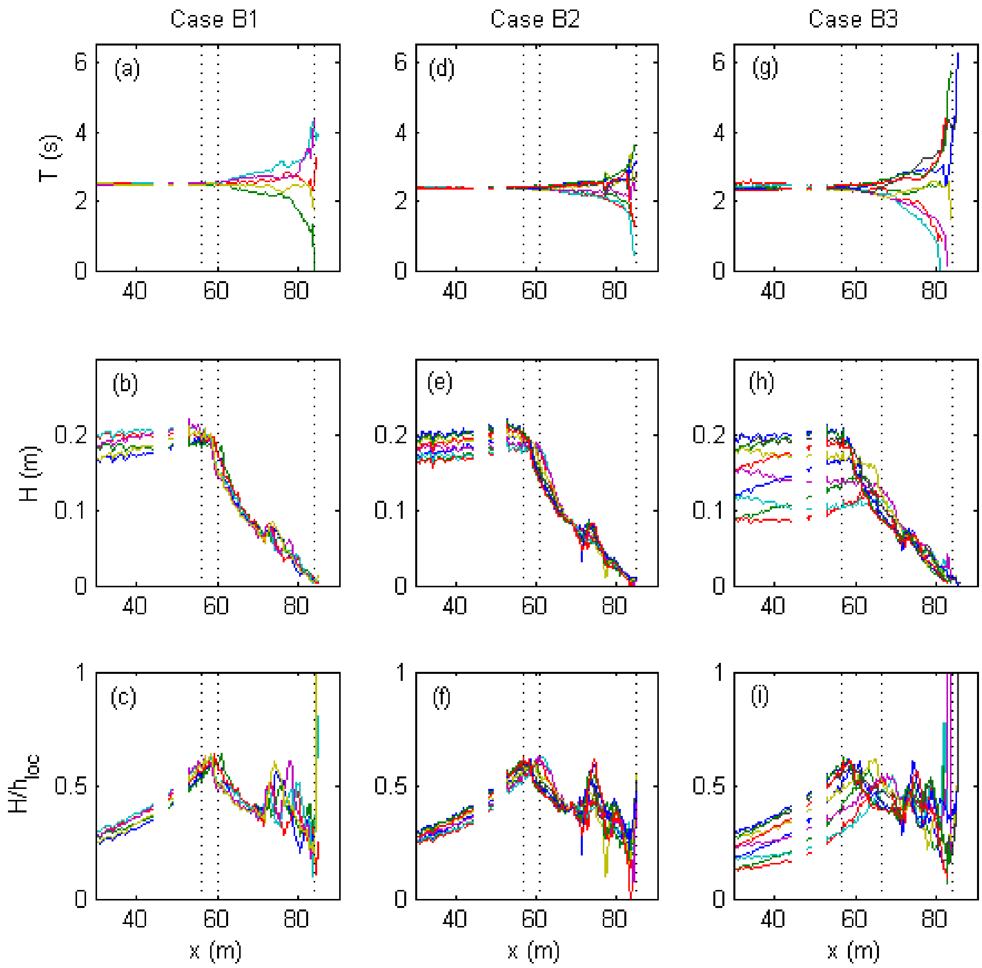

Figure 2: Short wave characteristics for cases B1 (first column), B2 (second column) and B3 (third column). (a),(d) and (g): individual wave periods; (b),(e) and (h): individual wave heights; (c), (f) and (i): relative wave height (H/h_{loc}). Vertical dotted lines: see Fig.1. For each case (column), one color corresponds to one given wave.

The cross-shore evolution of the individual wave heights is presented in Figures 2*b*, *e* and *h*. We can see that, as expected, the variability of the offshore wave height is much larger for case B3 than for cases B1 and B2. This results in larger variations of the breaking point location, which is in agreement with the positions determined visually during the experiment (vertical dotted lines). Once breaking is initiated, the scatter decreases quickly as wave heights become depth-limited. A local increase in the wave height can be observed at about 75 m for the three cases. It seems to correspond to the visual observations made during the experiment of a quasi-termination of breaking at about 70 m followed quickly by a reformation of the breaker (for almost all waves in cases B1 and B2, only for the smaller waves in case B3). Finally, the relative wave height is displayed in the bottom panels of Figure 2. It increases progressively during shoaling, until it reaches a value of 0.60-0.65. The relative water depth then decreases to a value of about 0.4, typical of the inner surf zone (e.g., Fig. 2*c*, $x\approx65$ m). More onshore, H/h_{loc} exhibits larger variations, which can be linked to the relatively larger infragravity-wave induced variations of water level. A peak of H/h_{loc} at $x\approx75$m (*e.g.*, Figs. 2*c*,*f*) can be also noticed, of amplitude similar to the one observed at the main breaking point. This seems to support the idea of a quasi-termination of breaking followed by the reformation of a new breaker.

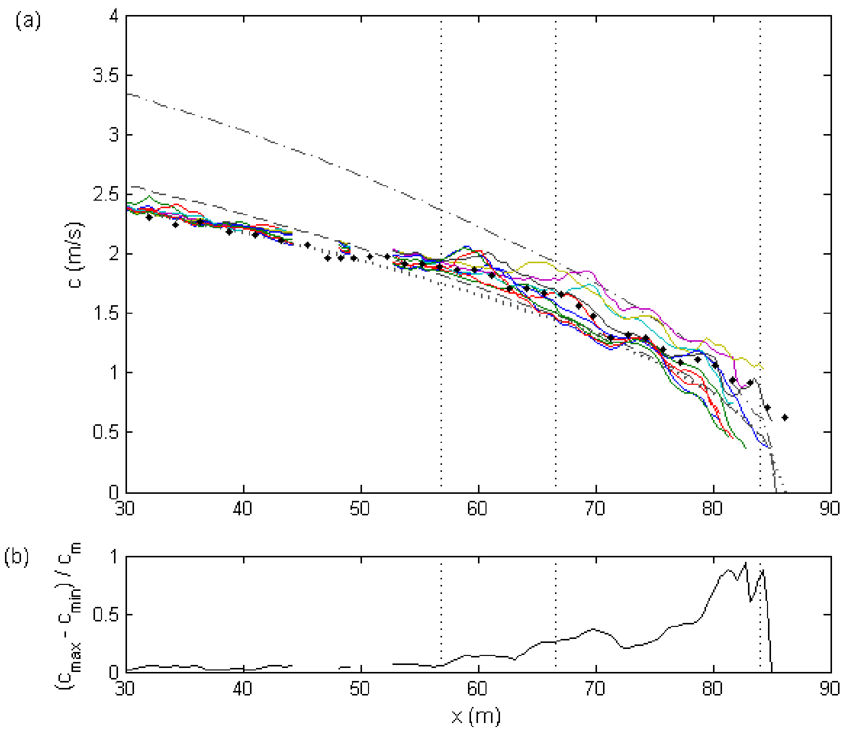

Figure 3: Intra-wave variability of the celerity for B3. (a) Individual wave celerity as a function of the cross-shore location. Dashed line: $c = (gh_m)^{1/2}$, dash-dotted line: $c=1.3(gh_m)^{1/2}$, dotted line: linear theory (dispersive). Black dots: celerity obtained by cross-correlation over 2 min-long signals; (b) $(c_{max} - c_{min})/c_m$, with c_{max}, c_{min} and c_m, the maximum, minimum and mean celerity at a given location. Vertical lines in (a) and (b): see Fig. 1.

3.2. ***Wave-by-wave celerity***

3.2.1. *Dispersion of individual wave celerity*

Figure 3*a* compares the individual wave celerity to 2-min averaged celerities obtained by cross-correlation (see Section 2.2 for details). This bulk celerity is very close to the values obtained after averaging the individual wave celerity (not shown), confirming the reliability of our methodology.

Before breaking, the celerity shows very little variability, and follows the linear dispersive relation (see thick dotted lines). The celerity of the individual waves start to differentiate at breaking. Wave breaking is associated with a strong steepening of the wave front: the crest is therefore accelerated forward, explaining the peak of celerity (defined as the crest celerity) following the initiation of breaking. This sharp increase at breaking is not found in the bulk estimate computed by cross-correlation, since it only gives an estimation of the celerity averaged over several waves. In the surf zone, the individual wave celerities exhibit variations up to 90% of the mean celerity c_m close to the swash zone (Fig. 3*b*), while these variations are less than 5% of c_m before breaking.

Figures 4*d* and 4*g* present the evolution of the wave-by-wave celerity for cases B1 and B2. For B1 and B2, the celerity goes down to the shallow-water linear theory (dashed lines) after breaking, and then increases again strongly. This could be in relation with the termination/restart of breaking mentioned earlier, and should be investigated in more detail based on the analysis of available video data. The different celerity curves finally diverge again when progressing toward the shore.

3.2.2. *Influence of the long waves*

The water level and velocity variations induced by the long waves are also shown in Figure 4. Some small discontinuities in the velocity signal can be observed, and can partly be explained by changes in the height

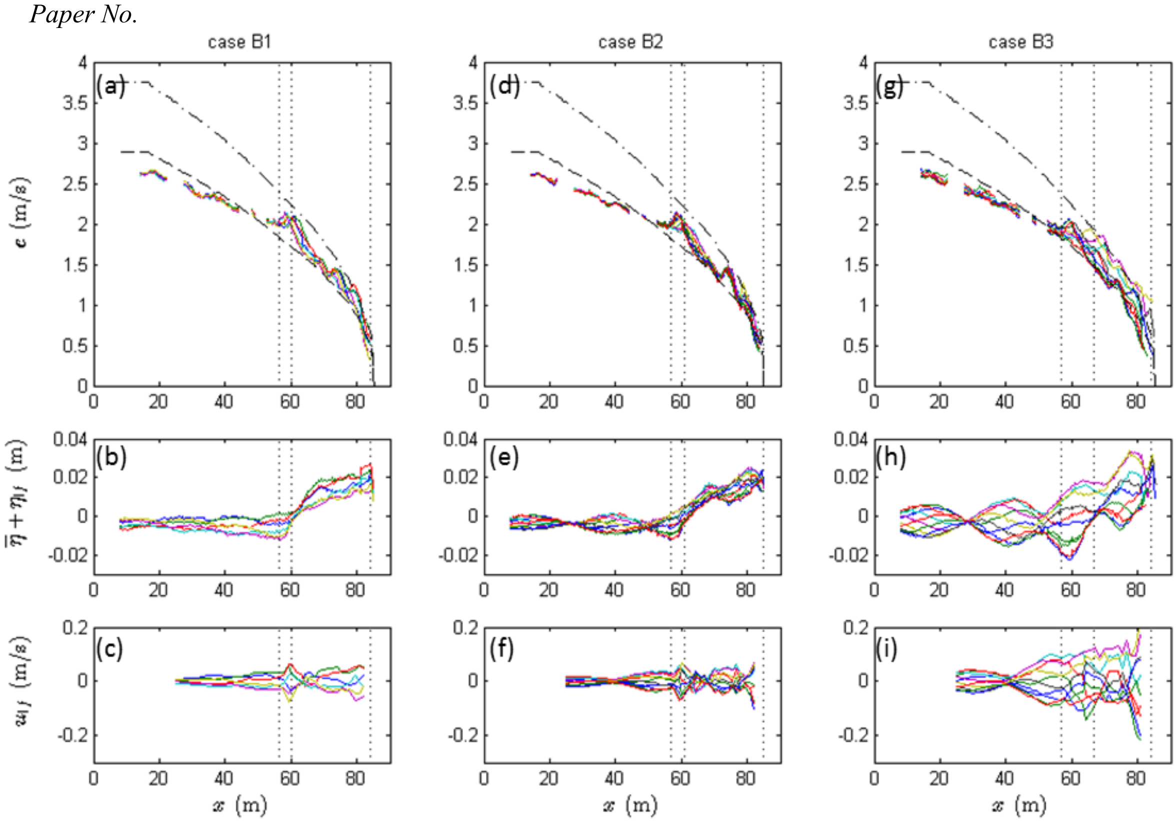

Figure 4: Top panel: individual wave celerity for the three cases. The dashed line is $(gh_m)^{1/2}$ with h_m the mean total depth obtained from averaging of the entire time-series, the dot-dash line is $1.3(gh_m)^{1/2}$; Middle and bottom panel: associated variation of the local free-surface elevation (set-up and influence long waves) and local velocity (long waves only) for each wave. Vertical dotted lines: see Fig. 1. For each column, one color corresponds to one given wave (same colors as Fig. 2).

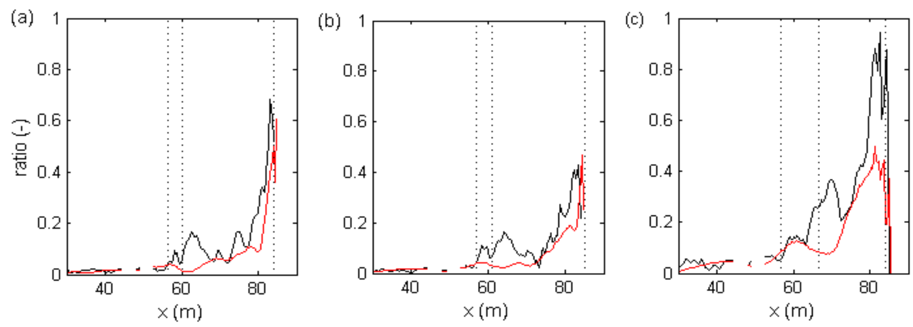

Figure 5: Evolution of $(c_{max} - c_{min})/c_m$ (back lines) and $(h_{loc,max} - h_{loc,min})/h_m$ (red lines) as a function of the cross-shore position x for the cases B1 (a), B2 (b) and B3 (c). $h_{loc,max}$, $h_{loc,min}$ and h_m are the maximum, minimum and averaged values of the water depth h_{loc} at a given location.

above the bed at which the measurements were obtained (see Ruessink *et al.*, 2013, their figure 1). A well-developed (anti-)nodal structure can be observed at the most offshore locations (x<50 m) in cases B2 and B3 for both the free-surface elevation and the velocity. As expected for a standing wave pattern, the nodes in free-surface (e.g., x≈30 m in Fig. 4h) correspond to the antinodes in velocity. It can be seen that for x<50 m, some waves are propagating alternatively close on the trough and on the crest of the long wave (η_{lf} negative or positive depending on the cross-shore location). No clear standing pattern can be observed in case B1, even at the most offshore locations. This can be explained by the higher value of f_2-f_1 considered in this case, which results in a higher dissipation of the long wave, and therefore a more onshore progressive pattern (see de Bakker *et al*., 2013 for a detailed analysis of long wave dissipation for the GLOBEX experiments).

In the surf zone, the long waves exhibit a more progressive pattern for the three cases. As a result, u_{lf} and η_{lf} can be maximum at the same time. This is expected to enhance the long-wave influence on short-wave celerity. To investigate these effects in more detail, we focus now on case B3, which exhibits the largest variations in terms of celerity but also the largest low-frequency modulations of water level and velocity. We can see in Figure 4, that, in the surf zone, the short waves with the largest celerities are those propagating in the largest water depths, that is to say on the long-wave crests (e.g., light green lines in Figs. 4, *g* and *h*). These waves are also propagating in a positive long-wave induced current (Fig. 4*i*). On the contrary, the waves propagating in the trough experience negative current and smaller water depths. They are therefore propagating at a lower speed than the waves on top of the crest. This leads to the convergence of the short waves on the long wave crest, and ultimately, to the merging of the bores (see trajectories of the wave crests in Fig. 1*b*).

Figure 5 compares the cross-shore evolution of the celerity ratio $\Delta c/c = (c_{\max} - c_{\min})/c_{\mathrm{m}}$ to the water depth ratio $\Delta h/h = (h_{\mathrm{loc,max}} - h_{\mathrm{loc,min}})/h_{\mathrm{m}}$. Before breaking, both ratios are close to zero. When the largest waves start breaking, a first increase in $\Delta c/c$ can be observed. It is followed by a second increase, starting after the second breaking point (breaking of the smallest waves). These two peaks cannot be related to local changes in water depth, but probably result from the strong steepening of the short wave following the initiation of breaking. Both ratios increase then at similar rate, except for the most shallowest locations, where the values of $\Delta c/c$ can be up to two times larger than $\Delta h/h$.

To analyze further the respective importance of the low-frequency variations of *u* and *h* on wave celerity, we show in Figure 6 the measured celerity as a function of the shallow water linear theory, computed using the mean water depth (blue dots), the local water depth (red dots) and finally the local water depth with an additional correction to account for the local current ($(gh_{loc})^{½} + u_{lf}$, green dots). In general, relatively small differences can be observed between the three celerity predictors. The largest differences are found for case B3, where accounting for the long-wave induced velocities reduces significantly the scatter of the celerity data for the shallowest positions (smallest *c,* Fig. 6c).

To quantify these differences, we define the following quadratic error:

$$E_{rms} = \sqrt{\frac{1}{N}\sum_{i=1}^{N}\left(\frac{c_{pred,i} - c_i}{c_i}\right)^2} \tag{2}$$

with $c_{pred,i}$ and c_i the predicted and measured celerities, respectively, and N the number of measurements. When considering the surf zone data only for the three cases (x>60m for B1 and B2, x>66m for B3, N=372 celerity values in total), we obtain a global E_{rms} of 11.5 % without velocity correction, and of 10.4% when accounting for the low-frequency variations of velocity. For B3 alone, E_{rms} = 10.1% when accounting for u_{lf}, and 13.2% otherwise.

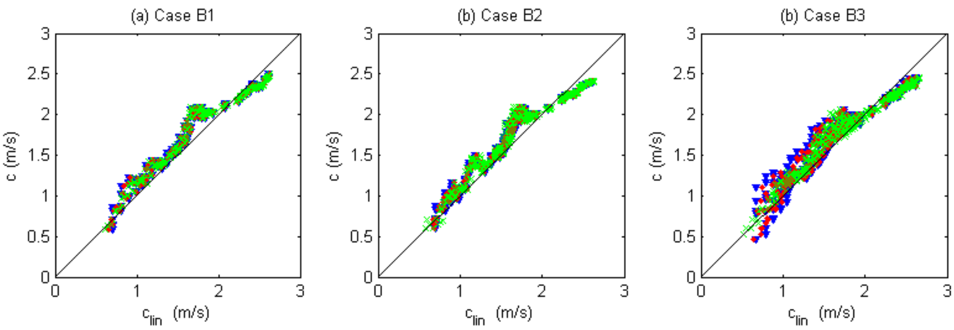

Figure 6: Individual wave celerity *c* as a function of the celerity predicted by the shallow water linear theory for the cases B1 (a), B2 (b) and B3 (c). Blue triangles: $c_{lin} = (g\ h_m)^{1/2}$, red dots: $c_{lin} = (g\ h_{\mathrm{loc}})^{1/2}$, green crosses: $c_{lin} = (g\ h_{\mathrm{loc}})^{1/2} + u_{\mathrm{lf}}$; Solid line: $c = c_{\mathrm{lin}}$; Note that only the data points corresponding to locations where both *h* and *u* were available (24.9 m<x<82 m) are plotted in this figure (no swash data).

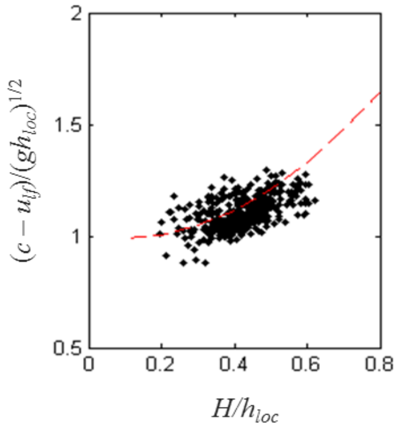

Figure 7: Normalized celerity $(c\text{-}u_{lf})/(gh_{\mathrm{loc}})^{1/2}$ as a function of the relative water depth for the surf zone data only (no points in the swash zone). Red line: best fit obtained for field data in Tissier et al. (2011).

3.2.3. *Non-linear effects*

Accounting for the low-frequency variations of water depth and velocity increases the agreement with linear theory in shallow water, but significant discrepancies still remain in the surf zone. In particular, we have seen that the linear theory generally underestimates individual wave celerity in the surf zone (see Fig. 6). Using the empirical modification of the linear theory $1.3(gh)^{1/2}$, arisen from laboratory experiments (Stive, 1984) and commonly-used in nearshore propagation models (Schaffer *et al.,* 1993), does not improve the predictions as E_{rms} = 20.3 % (see also dot-dash lines in Fig. 4a,d and g).
Previous studies emphasized the importance of accounting for wave amplitude in the calculations of broken wave celerity (among others, Thornton and Guza, 1982, Holland, 2001). In this section, we investigate the importance of finite-amplitude effects (or non-linear effects) on broken wave celerity. These can be quantified using the relative water depth, H/h_{loc}. Figure 7 represents the measured wave celerity normalized by the linear prediction as a function of the relative water depth for the surf zone data. It shows that the normalized celerity increases with increasing non-linearities. The red line in Figure 7 represents the polynomial fit defined in Tissier *et al.* (2011) for field celerity data of surf zone waves. Comparing our celerity data to this empirical fit leads to a root mean square error of 5.2%.

Lastly, we evaluate the ability of three non-linear predictors to describe broken wave celerity. The solitary wave model, although originally derived to describe non-breaking wave celerity, was historically the first model to account for non-linearities in wave propagation. In this case, wave celerity is predicted by:

$$c_{sol} = \left(g(\bar{h}+H)\right)^{1/2}, \quad (3)$$

with $\bar{h}$ the mean water level in which the waves propagate and H a representative wave height. The bore model, developed by Svendsen *et al.* (1978) , is based on the classical analogy between a broken wave and a hydraulic jump. Wave-front celerity is expressed as:

$$c_{bore} = \left(\frac{gh_t h_c (h_c + h_t)}{2\bar{h}}\right)^{1/2}, \quad (4)$$

where h_t and h_c are the water depth at the trough and at the crest. Finally, we consider the broken-wave celerity model introduced by Bonneton *et al.* (2004), which can be seen as a generalization of the bore model using Saint-Venant theory (hereafter called shock model). It reads as:

$$c_{shock} = -2\left(g\bar{h}\right)^{1/2} + 2\left(gh_t\right)^{1/2} + \left(\frac{gh_c}{2h_t}(h_t + h_c)\right)^{1/2}. \quad (5)$$

To evaluate the ability of these predictors to describe our wave celerity data, we choose $\bar{h} = h_{loc}$ and use the individual wave characteristics for h_t, h_c and H. Figure 8 compares the broken wave celerity to the predictions of the three non-linear model for the surf zone data. It can be seen that, as expected (*e.g.,* Thornton and Guza, 1982), the solitary wave model generally over-predicts broken wave celerity (Fig. 8*a*). For this model, we obtain a quadratic error of 10.1%, which is close to the values obtained using linear theory. The behavior of the bore and shock models are quite similar (Figs. 8*b* and *c*), even if it seems that the bore model performs slightly better for the highest celerity values. The resulting E_{rms} are close, 7.1% for the bore model and 7.5% for the shock model.

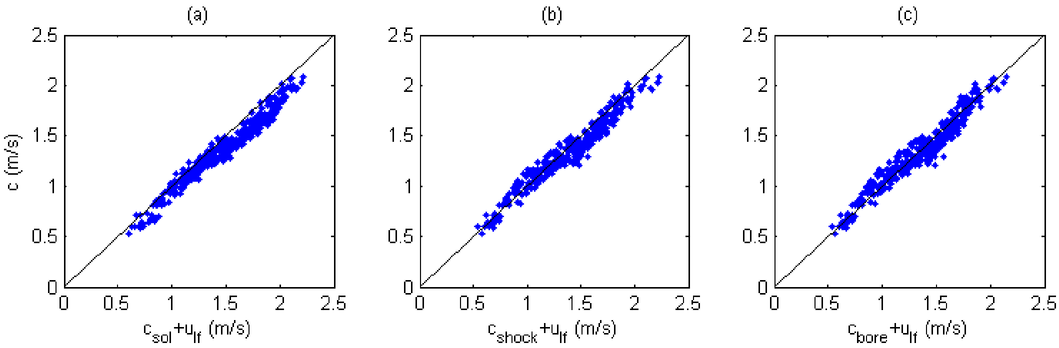

Figure 8: Comparisons of prediction versus measurements for the solitary wave (a), the shock (b) and the bore models (c). Surf zone data only.

4. Discussion and conclusion

In this paper, the wave-by-wave dynamics of surf zone waves has been analyzed in detail for three laboratory bichromatic conditions. We have shown that the individual wave celerity could exhibit variations up to 90% of the mean celerity over the duration of a wave group. The maximum variability is seen to relate with the relative long-wave surface elevation (with respect to the mean water depth), and is therefore maximum when approaching the swash zone. Moreover, individual short waves are seen to converge toward the long-wave crest while propagating through the surf zone. For the case B3, which is the case with the highest infragravity waves, it ultimately leads to the merging of several bores. This bore merging is enhanced by the fact that, for our laboratory conditions, both u_{lf} and h_{lf} are in phase in very shallow water (progressive pattern). Short waves propagating on the long-wave crests experience therefore higher water depths and positive long-wave currents, while those propagating on the long-wave trough propagate in smaller water depths and are slowed down by a negative long-wave current. This evolution would probably have been different in case of a (more classical) standing-long wave, since in this case u_{lf} and h_{lf} would be 90 degrees out of phase. This aspect will be investigated in more detail later on.

Several celerity predictors (linear and non-linear) have been evaluated. Surprisingly, the errors obtained while modeling individual waves are very close to those obtained by Tissier *et al.* (2011) for their field dataset using a bulk celerity number. The use of linear theory leads to an error of 10.4% when accounting for low-frequency variations of both the velocity and water level. The use of non-linear models improves the prediction, with quadratic errors of about 7% for both the bore and shock models. It is important to note that, in our study, most of the data points correspond to moderate values of the non-linear parameter (H/h<0.6), while the bore and shock models have been shown to differ the most for high non-linearities (Tissier *et al.*, 2011). Future works will include the analysis of the random wave cases, and in particular case A2 (see Ruessink *et al.*, 2012) which involves highly-energetic waves and strong non-linear interactions between short and long waves. The computation of individual wave celerity could be done using the Radon Transform methodology introduced in Almar *et al.* (2013), which is less subject to noise than our simple crest-tracking technique when applied to random wave cases.

Acknowledgements

Supported by the European Community's Seventh Framework Programme through the grant to the budget of the Integrated Infrastructure Initiative Hydralab IV, Contract no. 261520.

References

Almar, R., Cienfuegos, R., Gonzalez, E., Catalan, P.A., Michallet, H., Bonneton, P., Castelle, B., Suarez, L., Barred-beach morphological control on infragravity motion, *ICCE, Santander, Spain*, 2012.

Almar, R., Bonneton, P., Michallet, H., Cienfuegos R., Ruessink, G. and Tissier, M., 2013. On the use of the radon transform in studying wave dynamics, *Proceedings Coastal Dynamics,* 2013.

Almar, R., Bonneton, P., Sénéchal, N., Roelvink, D.A. Wave celerity from video imaging: a new method, *Proc. Int. Conf. Coast. Eng.*, ASCE 1, 661–673, 2008.

de Bakker, A., M. Tissier, V. Marieu, N. Sénéchal, A. Ruju, J. Lara and G. Ruessink, 2013. Infragravity-wave dissipation on a low-sloping beach. *Proceedings Coastal Dynamics* 2013.

Bonneton, P., Wave celerity in the surf zone, *Proc. Int. Conf. Coast. Eng.*, ASCE 1, 392–401, 2004.

Bonneton, P., Chazel, F., Lannes, D., Marche, F., Tissier, M., A splitting approach for the fully nonlinear and weakly dispersive Green-Naghdi model. *Journal of Computational physics*., 2011.

Catalán, P.A., Haller, M.C., Remote sensing of breaking wave phase speeds with application to non-linear depth inversions, Coast. Eng. 55 (1) 93–111, 2008.

Holland, T.K., Application of the linear dispersion relation with respect to depth inversion and remotely sensed imagery, *IEEE Trans. Geosci. Remote Sens.* 39 (9) 2060–2072, 2001.

Ruessink, B.G., Michallet, H., Bonneton, P., Mouazé, D., Lara, J.L., Silva, P.A., and Wellens, P., GLOBEX: Wave dynamics on a gently sloping laboratory beach, *Proceedings Coastal Dynamics,* 2013.

Schäffer, H., Madsen, P., Deigaard, R., A Boussinesq model for waves breaking in shallow water, *Coastal Eng.* 20 (3–4) 185–202, 1993.

Svendsen, I.A., Madsen, P.A., Hansen, J.B., Wave characteristics in the surf zone, *Proc. Int. Conf. on Coast. Eng.*, ASCE 1, 520–539, 1978.

Stive, M.J.F., Energy dissipation in waves breaking on gentle slopes, *Coast. Eng.* 8, 99–127, 1984.

Thornton, E.B., Guza, R.T., Energy saturation and phase speeds measured on a natural beach, *J. Geophys. Res.* 87 (C12) 9499–9508, 1982.

Tissier M., Bonneton, P., Almar, R., Castelle, B., Bonneton, N. and Nahon, A., Field measurements and non-linear prediction of wave celerity in the surf zone, *European Journal of Mechanics*, *B/ Fluid*, 2011.